

Lipid mapping in human dystrophic muscle by cluster-time-of-flight secondary ion mass spectrometry imaging

Nora Tahallah,* Alain Brunelle,* Sabine De La Porte,[†] and Olivier Lapr evote^{1,*}

Laboratoire de Spectrom trie de Masse,* Institut de Chimie des Substances Naturelles, Centre National de la Recherche Scientifique, Unit  Propre de Recherche 2301, F91198 Gif sur Yvette Cedex, France; and Laboratoire de Neurobiologie Cellulaire et Mol culaire,[†] Institut de Neurobiologie Alfred Fessard, Centre National de la Recherche Scientifique, FRC2118, Unit  Propre de Recherche 9040, F91198 Gif sur Yvette Cedex, France

Abstract Human striated muscle samples, from male control and Duchenne muscular dystrophy-affected children, were subjected to cluster-time-of-flight secondary ion mass spectrometry (cluster-ToF-SIMS) imaging using a 25 keV Bi₃⁺ liquid metal ion gun under static SIMS conditions. Spectra and ion density maps, or secondary ion images, were acquired in both positive and negative ion mode over several areas of 500 × 500 μm² (image resolution, 256 × 256 pixels). Characteristic distributions of various lipids were observed. Vitamin E and phosphatidylinositols were found to concentrate within the cells, whereas intact phosphocholines accumulated over the most damaged areas of the dystrophic muscles, together with cholesterol and sphingomyelin species. Fatty acyl chain composition varied depending on the region, allowing estimation of the local damage extent.—Tahallah, N., A. Brunelle, S. De La Porte, and O. Lapr evote. Lipid mapping in human dystrophic muscle by cluster-time-of-flight secondary ion mass spectrometry imaging. *J. Lipid Res.* 2008. 49: 438–454.

Supplementary key words Duchenne muscular dystrophy • human skeletal muscle degeneration • lipidomics • time-of-flight secondary ion mass spectrometry • oxidative stress • regeneration

First described by the French doctor Duchenne de Boulogne in the 19th century, Duchenne muscular dystrophy (DMD) is a severe degenerative genetic disease. Almost exclusively male children develop this myopathy, with an estimation of 1 in 3,500 boys worldwide (1). This X-linked recessive pathology is induced by the absence of expression or the truncation of dystrophin, a 427 kDa cytoskeletal protein involved in a transmembrane non-covalent complex of >20 proteins. The lack of dystrophin causes a rapid progression of skeletal, smooth, and cardiac muscle degeneration. The result, from the age of 2 or

3 years, is bad posture, unsteady gait, and difficulty in standing, walking, or climbing stairs. A wheelchair is necessary at ~10 to 12 years, and patients inexorably die around the age of 25–30 years. Dystrophin deficiency hampers the formation of an essential transmembrane complex that controls the integrity of muscle cell walls. This results in muscle cell membranes malfunctioning and membrane permeability, alteration of the ion drifts through the membrane (e.g., calcium), and oxidative stress. Diagnoses are based mainly on analyses of creatine kinase levels in the serum and electromyograms associated with biopsies or genetic tests. Among the therapies used to decelerate the damage caused by the disease are dystrophin-associated drug design, gene and cell therapies, and utrophin-associated therapies (2). To date, unfortunately, there is no cure for DMD.

In the last decade, research has been ongoing using different animal models (mice, dogs, cats, *Drosophila*, and *Caenorhabditis*) to gain a better understanding of the mechanisms of this lethal pathology. The dog model, closest to human, is rare and expensive, and although cheaper and more accessible, *Drosophila* and *Caenorhabditis* phenotypes are too different from the human one. The most widely studied model is the *mdx* (for X-linked muscular dystrophy) mouse, which develops unusually high concentrations of creatine and pyruvate kinases (3). The three advantages of the *mdx* mouse model are relatively low cost, good availability, and relatively short lifetime.

To gain more insight on DMD, our group previously carried out investigations on an *mdx* mouse leg muscle. Matrix-assisted laser desorption ionization-time-of-flight (MALDI-TOF) profiling (4) and cluster-time-of-flight secondary ion mass spectrometry (cluster-ToF-SIMS) imaging (5) were performed on 3 week old *mdx* mice as well as on

Manuscript received 24 September 2007 and in revised form 14 November 2007.

Published, JLR Papers in Press, November 17, 2007.
DOI 10.1194/jlr.M700421-JLR200

¹To whom correspondence should be addressed.
e-mail: olivier.laprevote@icsn.cnrs-gif.fr

Copyright ©2008 by the American Society for Biochemistry and Molecular Biology, Inc.

control (*nxtl*) and dystrophic (*xlt*) mouse myoblast cell cultures. These studies allowed us to distinguish three regions in the *mdx* mouse leg: a severely damaged region; a second region degenerating and undergoing oxidative stress and phosphatidylinositol (PI) cycle deregulation; and a third region that was stable.

Concerning ToF-SIMS, its input is continuously expanding in the field of lipidomics and drug/biomarker mapping on biological tissues at a micrometer scale (6). ToF-SIMS imaging has the major advantage, over alternative methods, of allowing direct and simultaneous collection of mass spectra and ion images. The determination of molecular composition and individual compound localization on a tissue section, at micrometer scale and without the need of any prior sample treatment, makes the analyses easier, more straightforward, and the closest possible to physiological conditions. Recent innovations, such as Bi_3^+ primary ion cluster sources (7), have tremendously enhanced the secondary ion emission yield of larger secondary ions. This development extended the capabilities of the method, rendering this approach particularly attractive and suitable for the investigation of biological tissues (8–16).

To validate the coupling of the ToF-SIMS imaging methodology with the *mdx* mouse model as a suitable approach for research on human pathology, we here report the first results obtained in human striated muscle sections and compare them with the previous outcomes in the *mdx* mouse. Cluster-ToF-SIMS imaging was used to map and characterize the molecular distribution in human control and dystrophic muscle tissue sections. Mass spectra revealed differences in the distribution of fatty acids, phospholipids, diglycerides (DGs), and triglycerides (TGs). Samples were analyzed in both positive and negative ion modes. The negative ion mode spectra displayed signals in the region m/z 200–350, corresponding to the palmitic (C16:0, m/z 255.2), palmitoleic (C16:1, m/z 253.2), stearic (C18:0, m/z 283.2), oleic (C18:1, m/z 281.2), linoleic (C18:2, m/z 279.2), and arachidonic (C20:4, m/z 303.2) fatty acid carboxylate (FA) ions. Between m/z 350 and 450, signals originated from cholesterol and α -tocopherol (vitamin E). Phospholipids and TGs were found between m/z 600 and 900. The DMD-affected muscles displayed different distributions of these ions in dystrophic cells and in severely damaged areas. Positive ion mode spectra confirmed the variation in intensity of cholesterol and vitamin E in the different areas. The proportion of phosphatidylcholines (PCs) also varied with the extent of degradation of the tissue. The ion images allowed us to differentiate the regions where the accumulation of these different compounds occurred in dystrophic cells, severely damaged areas, or adipocytes.

MATERIALS AND METHODS

Surgery residues of human paravertebral striated muscles from male control and DMD-affected 12 to 14 year old children were provided by the Banque de Tissus pour la Recherche

(Institut de Myologie Hôpital de la Pitié-Salpêtrière, Paris, France) after approval of the project (by decision on December 14, 2004).

Histological staining

Ten micrometer thick sections were cut at -20°C in a CM3050-S cryostat (Leica Microsystems SA, Rueil-Malmaison, France) and immediately deposited onto a glass plate and stored at -80°C for histological staining. The dystrophic appearance of the human paravertebral striated muscle was studied with Masson's trichrome staining (Sigma kit No. HT15) to visualize muscle fibers (in red), connective tissue, and collagen (colored by the aniline blue). Histological images were taken with a DMRXA2 microscope (Leica Microsystems SA).

Sample preparation for cluster-ToF-SIMS imaging

Cryostat sections (20 μm) were prepared, placed on glass plates, and briefly stored at -80°C . Immediately before analyses, samples were dried under a few millibars of pressure for 30 min without any further treatment. Then, images were recorded with an Olympus BX51 microscope (Rungis, France) equipped with 1.25 \times to 50 \times lenses and a Color View I camera (Soft Imaging System) and monitored with Olympus DP Soft software.

ToF-SIMS data acquisition and processing

All experiments were performed on a commercial ToF-SIMS IV (ION-TOF GmbH, Münster, Germany) reflectron-ToF mass spectrometer located at the French Institut de Chimie des Substances Naturelles in Gif-sur-Yvette. The instrument was fitted with a Bi_3^+ cluster ion source at a 45° incidence angle. The primary ion dose density was 2×10^{11} ions/ cm^2 for each ion mode, with a 150 μs cycle time and a 0.27 pA measured pulsed current. The ion column focusing mode ensured both a 1–2 μm beam focus and a high mass resolution, which is a prerequisite for accurate mass measurements and assignments. A low-energy electron flood gun neutralized the surface during analysis. The secondary ions were first extracted with 2 keV kinetic energy, had an effective ion flight path of ~ 2 m, and were then postaccelerated to 10 keV before hitting the detector surface. The sample surface was directly observable through an integrated video camera. Positive and negative secondary ion images, obtained with IonImage software, had a field of view of $500 \times 500 \mu\text{m}^2$ (256×256 pixels). Images were compressed during data processing to 128×128 pixels to increase the contrast, leading to a final lateral resolution of 4 μm . For more clarity, images were also averaged and rescaled. To ensure the correct localization on each spot, a thorough examination was performed for each compound: an image was generated for each peak of the isotopic distribution of the compound (i.e., for the ^{12}C atom-containing peak, for the $^{13}\text{C}_1$ -containing peak, and for the peak containing two ^{13}C atoms). These images were then matched and summed to obtain the final compound image. However, in cases like that of PC34:2 (see the section on isotopic correction below for details), only the first two images were summed. Subsequently, regions of interest (ROIs) were manually selected and the corresponding mass spectra were extracted to obtain local information. These selected regions may have different areas. Therefore, and for a proper comparison, the spectrum corresponding to each ROI needed to be normalized against the area of the smallest one. In the following, the selected cells and intercellular and damaged areas are characteristic of all the different types of cells and intercellular and damaged areas contained in the analyzed sections.

Calibration and mass assignments

The method used was the same as that described in Ref. 5. The very low initial secondary ion kinetic energy (17) allows a linear relationship between the time of flight and the square root of m/z over the whole mass range. Therefore, an internal calibration is possible using the signals of H^+ , H_2^+ , H_3^+ , C^+ , CH^+ , CH_2^+ , CH_3^+ , trimethylammonium ($C_3H_{10}N^+$; m/z 60.08), a choline fragment ($C_5H_{12}N^+$; m/z 86.10), choline ($C_5H_{14}NO^+$; m/z 104.10), and PC ($C_5H_{15}O_4NP^+$; m/z 184.07) for the positive ion mode and the signals of C^- , CH^- , CH_2^- , C_2^- , C_3^- , C_4H^- , PO_2^- (m/z 62.96), PO_3^- (m/z 78.96), and $H_2PO_4^-$ (m/z 96.97) for the negative ion mode. Signals of the fatty acid carboxylate ions and vitamin E deprotonated molecule were used for the negative ion mode calibration refinement. For the positive ion mode, cholesterol fragment and deprotonated molecule, deprotonated vitamin E, and DG fragment signals were selected. Because of the lack of an efficient MS/MS method that could be associated with TOF-SIMS imaging, structure attributions or assignments of ion peaks were made according to the instrument resolution and accuracy, the valence rule, and the biological characteristics of the tissue, as mentioned in Ref. 5. Many mass assignments have also been confirmed or at least reinforced with the help of the literature. Details are given below.

Calculation of lipid intensity ratios with isotopic correction

In this report, the intensity refers to the area of the ion peak in the corresponding mass spectrum. Large mass lipids (e.g., PCs) contain an important number of carbons. Therefore, the positive ion mode PC34:2 signal is composed of 60.7% monoisotopic peak (m/z 758.6), 29.5% $^{13}C_1$ -containing ions (m/z 759.6), and 8% two ^{13}C atoms (m/z 760.6). This latter peak thus contributes to the intensity of the PC34:1 monoisotopic peak at m/z 760.6. Additionally, the emission yields and detection efficiencies for compounds of the same family and close molecular weight are considered equivalent (18). Hence, when calculating PC intensity ratios, the isotopic contribution correction has been applied. For the sake of precision, the calculation of fatty acids intensity ratios, in negative ion mode, was also performed by taking into account this same correction.

Definitions of ratios

$R_1 = I_{m/z\ 758}/I_{m/z\ 760}$. R_1 is the ratio of the intensity of the PC34:2 protonated molecule signal at m/z 758.6 over the corrected intensity of the PC34:1 protonated molecule signal at m/z 760.6 in the positive ion mode. $R_2 = I_{m/z\ 283}/I_{m/z\ 281}$. R_2 is the ratio of the corrected intensity of the C18:0 fatty acid carboxylate signal at m/z 283.2 over the intensity of the C18:1 fatty acid carboxylate signal at m/z 281.2 in the negative ion mode. $R_3 = I_{m/z\ 281}/I_{m/z\ 279}$. R_3 is the ratio of the corrected intensity of the C18:1 fatty acid carboxylate signal at m/z 281.2 over the intensity of the C18:2 fatty acid carboxylate signal at m/z 279.2 in the negative ion mode.

RESULTS

We investigated human striated muscle originating from surgery residues of one control (12 year old) and two DMD-affected (13 and 14 year old) children. Four cryosections from the control and two sections from each DMD-affected muscle were selected. On each section, two to six zones were subjected to ToF-SIMS imaging. These 33 ToF-SIMS-analyzed zones (13 control and 20 dystrophic) will be referred to as spots here for clarity.

Figure 1A shows the microscope optical image of a section from the control 12 year old child surgery residue. In green is delimited spot 1, one of the areas subjected to ToF-SIMS analyses. Individual, compact, and regular myofibers (muscle cells) are visible, all sheathed by a membrane in whole fascicles. Figure 1B displays the microscope optical image of a section from a 14 years old DMD-affected child surgery residue; in green are highlighted two of the analyzed spots (2 and 3) described in this report. Physical differences are visible between nonstruc-

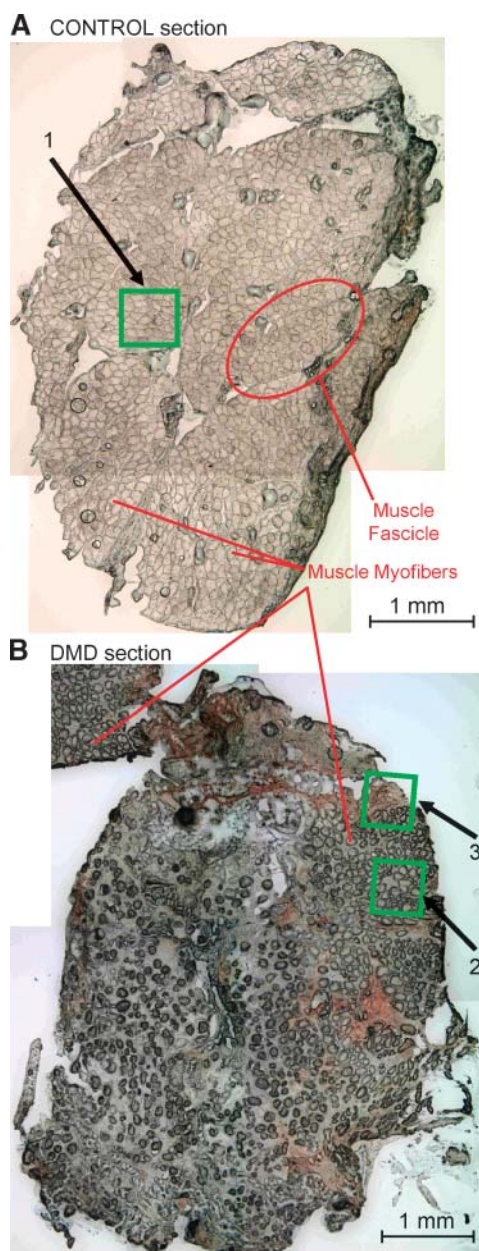


Fig. 1. Microscope images of 20 μ m thick sections of human striated muscle surgery residues before time-of-flight secondary ion mass spectrometry (ToF-SIMS) analyses. Some of the analyzed spots are delimited by the green squares. A scale is shown at the bottom of each image. A: Control section. B: Duchenne muscular dystrophy (DMD)-affected section.

tured, damaged, and pseudohealthy zones. The colors vary, and the fibrous membrane sheaths are absent. Although the myofibers are clearly observed, they are not regularly sized and only a few zones appear more compact. Finally, these two images helped us to choose the areas to be analyzed by mass spectrometry imaging on the DMD-affected muscle sections.

Histology of control and DMD-affected human striated muscle sections

As a start, to probe the physiological status of the muscles and visualize connective tissue, muscle fibers, and collagen, we applied to control and dystrophic human striated muscle sections Masson's trichrome staining. The healthy muscle fibers in **Fig. 2A** appear (in red) regular, compact within a fascicle membrane, and surrounded by only a minute amount of collagen (in blue). Conversely, the DMD-affected muscle cells (**Fig. 2B**) are irregular, dislocated, lacking fascicle membrane, and surrounded by an important amount of collagen and connective tissue within the numerous damaged areas.

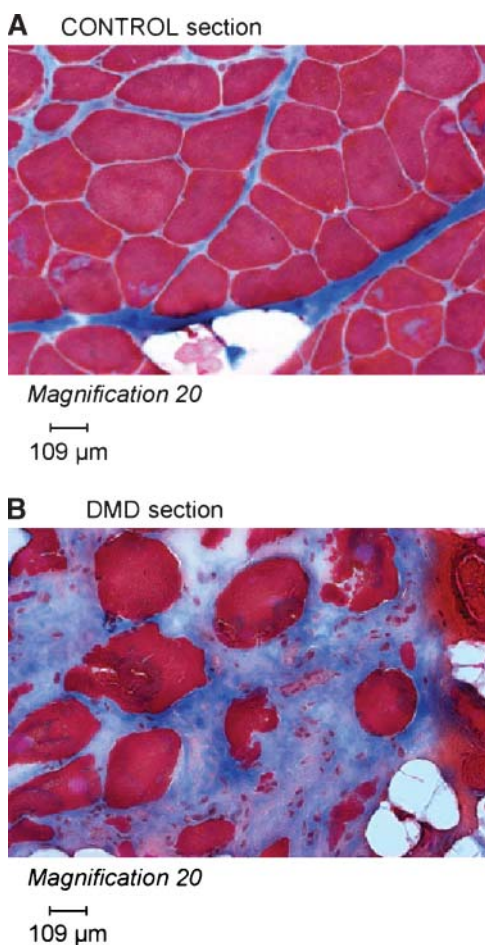


Fig. 2. Trichrome Masson histological staining of 10 μm thick muscle sections. Red indicates cytoplasm, and blue indicates collagen. A: Control section. B: DMD-affected section.

ToF-SIMS spectrum from a control muscle section

A control human striated muscle was first analyzed by ToF-SIMS imaging (e.g., spot 1; **Fig. 1A**). The total mass spectrum of spot 1 recorded in positive ion mode is displayed in **Fig. 3** (m/z range 80–820). Choline and PC fragment ions at m/z 86.1, 104.1, 125.0, and 184.1 have been identified by other authors, and their structures are given in Ref. 4, whereas the PC fragment ion at m/z 224.1 has been identified by ToF-SIMS postsource decay measurements directly on a rat brain section (19). The cholesterol ions, at m/z 369 and 385 in positive ion mode, have been already mentioned in many papers (10, 11, 20). Positive ions of vitamin E have been identified in previous imaging experiments (5, 12). Series of positive ions are observed in the m/z 500–620 range. These ions are likely to be fragments of DGs, TGs, PCs, or PIs. These ions are labeled with the generic name “DG-type fragment.” Their ion images (data not shown) reveal a general colocalization with TGs, suggesting that these DG-type fragment ions originate mainly from the fragmentation of DGs and TGs. PC-positive ions in the region m/z 750–810 have been observed and characterized in ToF-SIMS imaging experiments by several authors (5, 10, 11). In particular, the structures of these ions have been studied directly from mouse muscular cell cultures by MALDI-ToF tandem mass spectrometry (4). Finally, the ion detected at m/z 723.5 might tentatively be attributed to a sodiated sphingomyelin (SM) ion.

Like the mouse samples, the human muscle sections also exhibit intact PC ions as the dominant species in the region m/z 650–820, principally PC34:2 and PC34:1 (m/z 758.6 and 760.6, respectively), and their respective sodium adducts at m/z 780.6 and 782.6 and potassium adducts at m/z 796.6 and 798.6. It must be mentioned that PC34:2 and PC34:1 ions are not the only PC ions that are detected. Several other PC ion species are also present in the spectra, as was the case for the previous studies in the mouse model (4, 5). PC fragments appear in the region m/z 80–300.

ToF-SIMS imaging of PCs

Figure 4A depicts, from left to right, the microscope image of spot 1, the images of the m/z 758 and 760 ions over the analyzed surface, and the selected ROIs. Indeed, ToF-SIMS imaging gives the opportunity to select particular ROIs on the analyzed surface and to extract, from each of them, the corresponding spectrum. Therefore, to obtain more precise information, we selected different ROIs within spot 1 (**Fig. 4A**, right), driven by the different distributions on the ion images. In red, green, and blue are shown selected cells, and in pink is an intercellular space. From each ROI a mass spectrum was extracted, as shown in **Fig. 4B**, and the corresponding PC34:2/PC34:1 (758.6/760.6) intensity ratio was calculated. For the sake of clarity, this ratio is referred to as R_1 below. Most of the selected regions led to an R_1 value of ~ 2 (**Fig. 4C**). By contrast, a unique cell (selected in green) gave R_1 at 0.80. The ion images (**Fig. 4A**) pointed as well to this cell as the

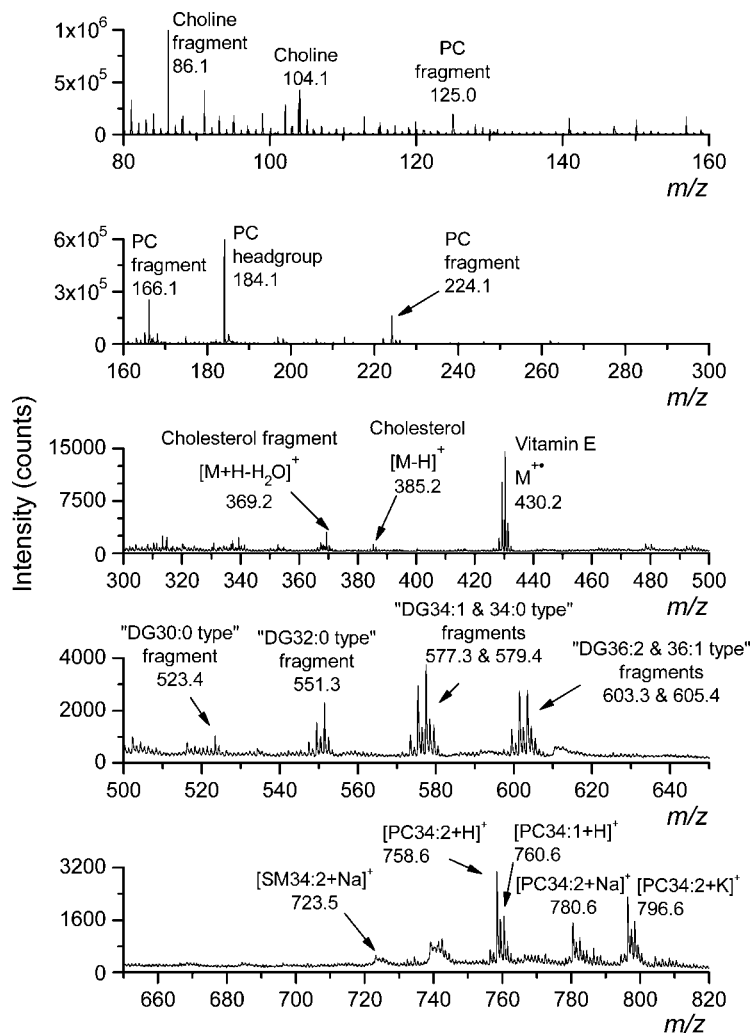


Fig. 3. ToF-SIMS total mass spectrum of spot 1 (control; see Fig. 1A) in positive ion mode. DG, diglyceride; PC, phosphatidylcholine; SM, sphingomyelin.

only area where the m/z 758 ion intensity is clearly lower than the m/z 760 ion intensity. If the present results are to be compared with those obtained from the *mdx* mouse model (4), this means that this might be a regenerating cell.

We then analyzed the different DMD-affected muscle sections, and the results are illustrated by two typical examples in Figs. 5 and 6. A first pseudohealthy region, containing almost exclusively highly uniform and compact cells, drew our attention (Fig. 5). We focused on this spot (spot 2 in Fig. 1B) to start the comparison between the control and DMD-affected samples. The value of R_1 , for the whole spot 2, was 1.27 (Table 1, DMD section 1), in accordance again with the *mdx* mouse model. However, the mass spectra (Fig. 5B) corresponding to the selected ROIs (Fig. 5A, right) and the R_1 values of the different ROIs reported in Fig. 5C showed that the cells were not fully identical, in terms of PC composition, over this zone. Indeed, the small cells (blue ROI) exhibited an R_1 value of 1.26. However, the larger cells split in two: some cells (in red) generated a ratio value of 1.21, similar to the small cells, whereas others (in green) gave an R_1 value of 1.42. The large cells delimited by the green ROI then presented a PC composition similar to that of the healthy tissue,

whereas the intercellular space ($R_1 = 0.71$) behaved like a regeneration zone. The big cells in the red ROI and the small cells in the blue ROI appeared to be in an intermediate state.

The second characteristic region of the DMD-affected human muscle is typified by spot 3 (Fig. 1B). The R_1 global value for this spot was determined to be 1.13 (Table 1, DMD section 1), suggesting an m/z 758.6 ion slightly more abundant than the m/z 760.6 ion. Figure 6A depicts, from left to right, the microscope image, the images of the ions at m/z 758 and 760, and the selected ROIs over spot 3. For more detailed information, we chose ROIs corresponding to three morphologically different regions (Fig. 6A, right): relatively ordered cells were selected in red, a damaged area in green, and some adipocytes in blue. Figure 6B shows the mass spectra of each of these selected ROIs (m/z 650–820), whereas Fig. 6C displays the corresponding R_1 values (1.04 within the cells and 0.83 in the damaged region). In the mass spectrum of the blue ROI (adipocytes), the signal-to-noise ratio was not sufficient to determine the R_1 . Thus, in DMD spot 3, the relatively ordered cells exhibit similar behavior to that of the control zones in the *mdx* mouse model. On the other hand, the damaged area generated an R_1 value of 0.83, corresponding to that of the

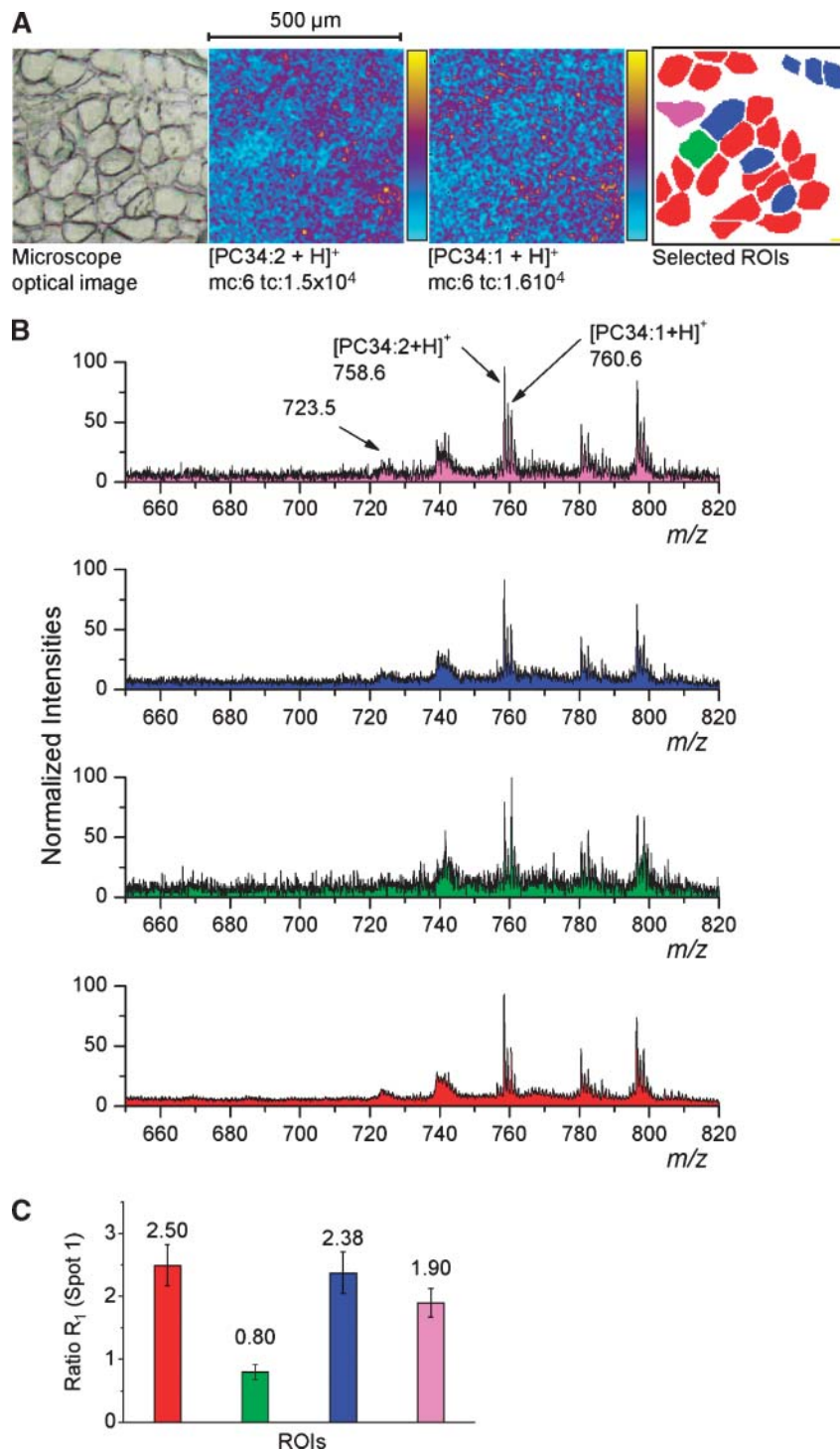


Fig. 4. ToF-SIMS analysis of spot 1 (control; see Fig. 1A) in positive ion mode. A: From left to right: microscope image; m/z 758 and 760 ion images with maximal number of counts in a pixel (mc) for the color scale and image total number of counts (tc), field of view $500 \times 500 \mu\text{m}^2$, compressed to 128×128 pixels, averaged and rescaled; and selected regions of interest (ROIs; red, green, and blue indicate cells, and pink indicates intercellular space). B: m/z 650–820 enlargement of each ROI's spectrum. C: R_1 (758:760) ratio for each selected ROI. Error bars indicate \pm SEM.

intercellular region of DMD spot 2 and to the green cell of control spot 1. Similar to the destructured (regenerating) zone in the *mdx* mouse model, these ratio values were <1 . This could denote an intensive regenerating activity

and not degeneration, as would be expected from the color, aspect, and absence of fascicles on the microscope image of spot 3. Additionally, compared with spot 2, the lower R_1 produced by the cells of spot 3 indicates that

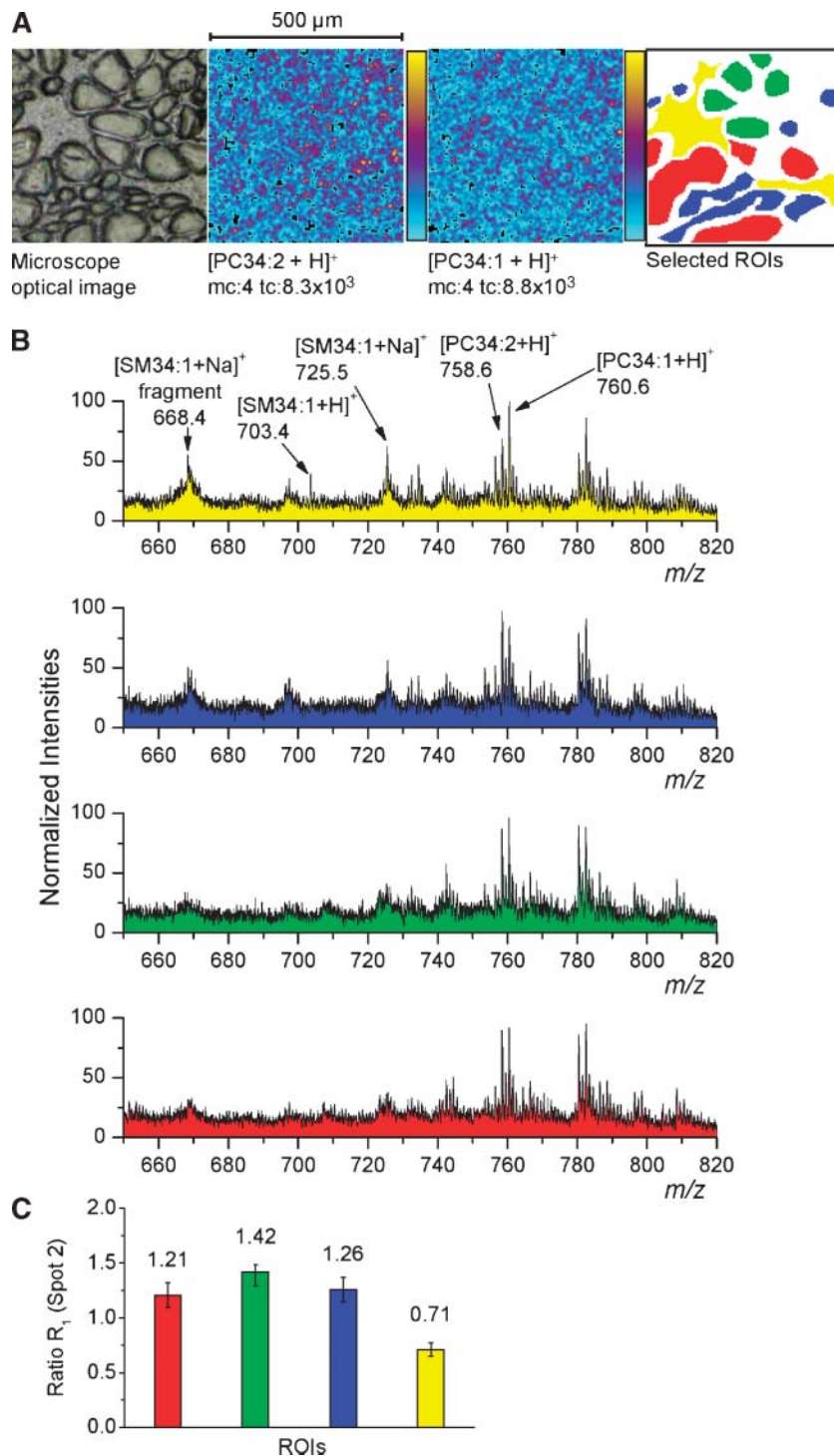


Fig. 5. ToF-SIMS analysis of spot 2 (DMD; see Fig. 1B) in positive ion mode. A: From left to right: microscope image; m/z 758 and 760 ion images with maximal number of counts in a pixel (mc) for the color scale and image total number of counts (tc), field of view $500 \times 500 \mu\text{m}^2$, compressed to 128×128 pixels, averaged and rescaled; and selected ROIs (red, green, and blue indicate cells, and yellow indicates intercellular space). B: m/z 650–820 enlargement of each ROI's spectrum. C: R_1 (758:760) ratio for each selected ROI.

these cell PCs have incorporated less C18:2, as observed previously in DMD-affected human muscles (21, 22). This also means that spot 2 is in a more stable state than spot 3 and confirms the pseudohealthy nature of spot 2.

The reproducibility of these results was verified on different sections of the same (control and dystrophic) surgery residues, and their reliability was validated on sections of a second dystrophin-deficient child surgery residue.

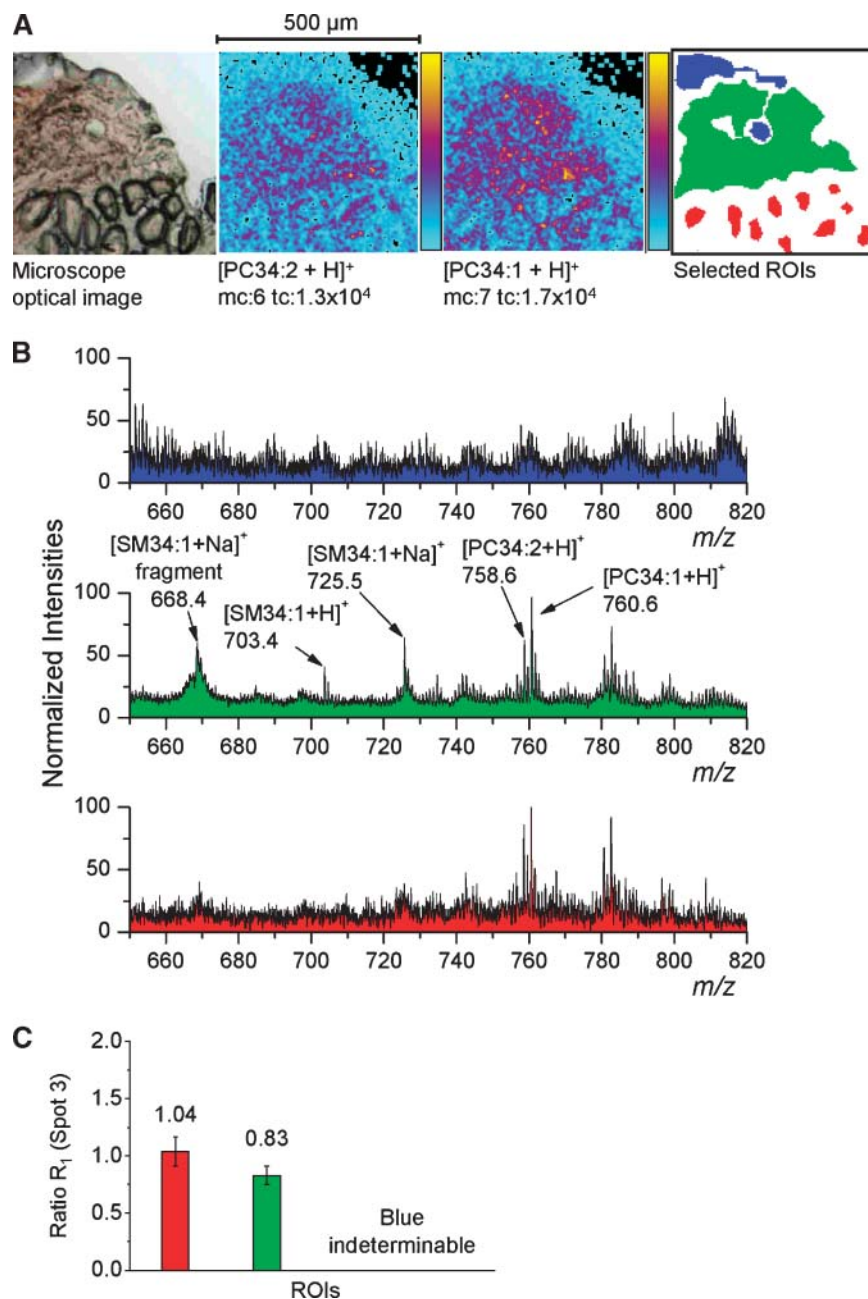


Fig. 6. ToF-SIMS analysis of spot 3 (DMD; see Fig. 1B) in positive ion mode. A: From left to right: microscope image; m/z 758 and 760 ion images with maximal number of counts in a pixel (mc) for the color scale and image total number of counts (tc), field of view $500 \times 500 \mu\text{m}^2$, compressed to 128×128 pixels, averaged and rescaled; and selected ROIs (red indicates cells, green indicates damaged area, and blue indicates adipocytes). B: m/z 650–820 enlargement of each ROI's spectrum. C: R_1 (758:760) ratio for each selected ROI.

Table 1 summarizes the global R_1 calculations performed on all control and dystrophic muscle sections. The control samples provided an average ratio value of 1.85 (± 0.31 SD), higher than that found for the healthy and control areas of the mouse model (4). For the dystrophic samples, the R_1 average value was calculated to be 1.15 ± 0.17 , rather comparable to that found for healthy and control areas of *mdx* mouse. The data shown here match the results of intensity ratios between m/z 758.6 and 760.6

for healthy and dystrophic cells on day 1 of culture (myoblasts) in Ref. 4.

ToF-SIMS imaging of cholesterol and SM

A remarkable feature in the m/z 650–820 region is the presence of three signals that we tentatively attributed to the SM species: SM34:1 (d18:1/16:0) and SM34:2 (d18:1/16:1 or d18:2/16:0). The mass spectrum of a DMD sample

TABLE 1. R_1 ratios calculated for each control and dystrophic spot

Sample	Section Number	Spot Number	Spot Ratio R_1	Section Average Value	SD	Sample Average Value	SD
DMD child 1	1	1	1.13	1.00	± 0.11	1.15	± 0.17
		2	1.27				
		3	1.13				
		4	0.99				
		5	1.13				
	2	1	0.84	1.13	± 0.11		
		2	1.04				
		3	0.90				
		4	1.14				
		5	1.08				
DMD child 2	3	1	1.54	1.32	± 0.19		
		2	1.42				
		3	1.07				
		4	1.37				
		5	1.20				
	4	1	1.25	1.16	± 0.13		
		2	1.23				
		3	0.94				
		4	1.18				
		5	1.19				
Control	1	1	1.89	1.96	± 0.22		
		2	1.82				
		3	1.73				
		4	2.22				
		5	2.16				
	2	1	2.06	2.17	± 0.16		
		2	2.28				
	3	1	1.79	1.63	± 0.36		
		2	1.89				
		3	1.22				
	4	1	1.99	1.65	± 0.29		
		2	1.50				
		3	1.47				

DMD, Duchenne muscular dystrophy. $R_1 = I_{m/z\ 758}/I_{m/z\ 760}$; ratio of the intensity of the PC34:2 protonated molecule signal at $m/z\ 758.6$ over the corrected intensity of the PC34:1 protonated molecule signal at $m/z\ 760.6$. Data originate from positive ion mode time-of-flight secondary ion mass spectrometry (ToF-SIMS) analyses of four human striated muscle sections from a control child and two sections from two DMD-affected children. The spots correspond to areas over which ToF-SIMS imaging experiments were carried out.

(Fig. 7A, lower spectrum) indeed showed peaks corresponding to the protonated molecule ($m/z\ 703.5$, $[\text{SM}34:1+\text{H}]^+$), to the sodium adduct ($m/z\ 725.5$, $[\text{SM}34:1+\text{Na}]^+$), and to a fragment possibly corresponding to the choline head group elimination from the sodiated lipid ($m/z\ 668.4$). These ions have been described in the literature for membrane sphingolipids (23), which have been reported to be involved in the activation of ion channels and functional rafts (24, 25) and to be colocalized with them (26). SMs are now known to colocalize with cholesterol and to form rafts in plasma membranes of cultured cells (27, 28), and PCs and cholesterol have been found to interact in membrane bilayers (28, 29). The ion images of spot 3 revealed a maximum of cholesterol species (Fig. 8A) and SM species in the damaged region, together with PC34:2 and PC34:1 (Fig. 8B). For the pseudohealthy spot 2, a maximal accumulation of SM and cholesterol species was found in the intercellular region. The other analyzed spots confirmed their colocalization in intercellular or damaged areas. It is noteworthy that, in spot 2, some SM species were also present in the small cells, unlike in the large cells. For the control spot 1, practically no SM ion was detected except the $m/z\ 723.5$ species, tentatively assigned to the sodiated SM34:2, which gave some signal all over the spot sur-

face (data not shown), together with ions at $m/z\ 758.6$ and 760.6 . In this sample, cholesterol accumulated only in intercellular spaces or adipocytes but not in cells.

ToF-SIMS spectra of fatty acids

The mass spectra recorded in the negative ion mode (enlargement $m/z\ 240\text{--}320$) of control and dystrophic muscles are displayed in Fig. 7B. Distributions appear distant of 28 mass units with peaks separated by 2 mass units, characteristic of fatty acid carboxylate ions with different chain lengths bearing a variable number of double bonds (5). In control and DMD-affected samples, the same series of fatty acid ions were present. However, their intensities varied according to the nature of the sample.

Table 2 summarizes the global fatty acid abundance ratio R_2 (C18:0/C18:1) for each analyzed spot of the control and dystrophic muscles, calculated as described in Materials and Methods. The control sample spots exhibited an average ratio (0.77 ± 0.16) that was ~ 1.5 times higher than that of the dystrophic cells (0.54 ± 0.14). These values significantly depended on the relative abundance of the cells in the spot area. A more thorough examination of the different ROI ratios within each DMD-affected spot showed that the cells presented R_2 values of

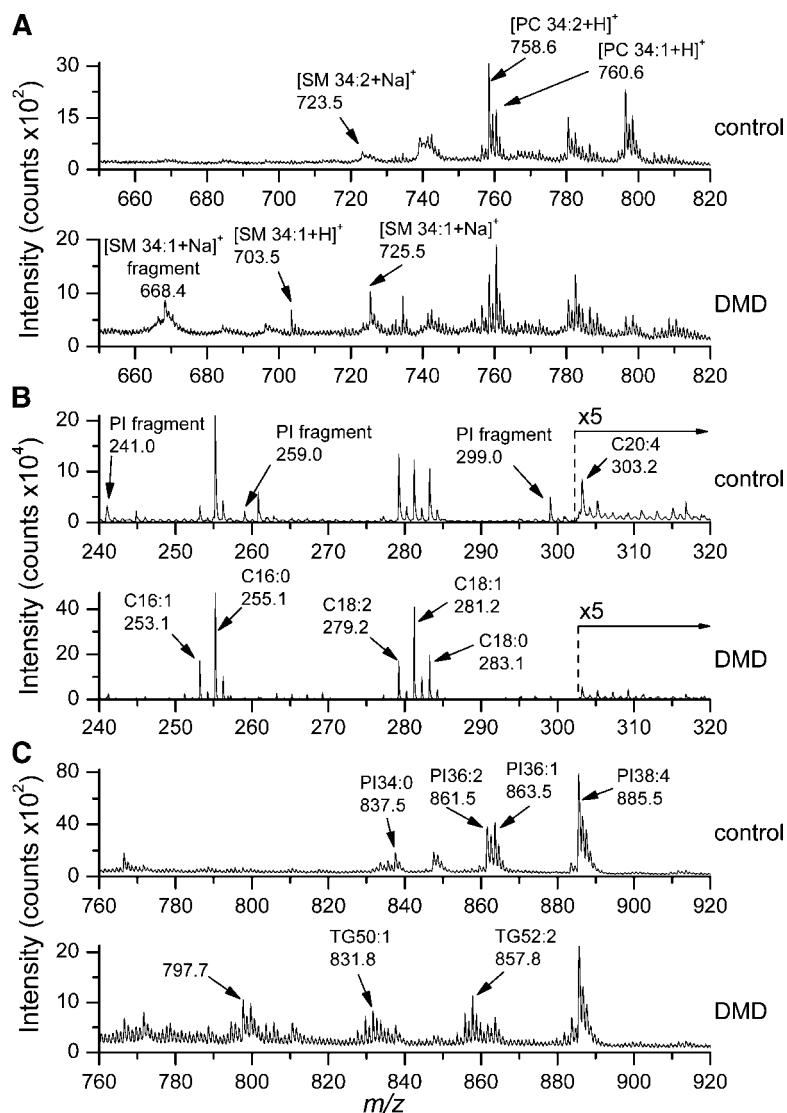


Fig. 7. ToF-SIMS global spectra of control and DMD-affected striated human muscle sections. A: Positive ion mode: m/z 650–820 mass range (PCs and SMs). B: Negative ion mode: m/z 240–320 (fatty acid carboxylate ions). C: Negative ion mode: m/z 760–920 [PCs and triglycerides (TGs)].

0.6–0.9 (i.e., higher than the average value). In other words, for the DMD-affected sections, the higher global ratios (~ 0.7) corresponded to pseudohealthy regions and to spots containing healthier cells. The lower ratios were obtained from the most damaged spots (~ 0.3). The DMD intercellular or damaged regions gave R_2 values of 0.4–0.5 versus ~ 0.8 for the control intercellular regions. The adipocytes in dystrophic spot 3 exhibited a ~ 0.4 R_2 value as well.

An additional striking feature is the generally high level of C18:2 in the control human muscle (Fig. 7B). In **Table 3**, an average value of 0.98 ± 0.18 was calculated for the R_3 (C18:1/C18:2) in the control samples, whereas it reached 1.96 ± 0.44 for the dystrophic muscles. Hence, this ratio might also be an indicator of the DMD disease, because the control average R_3 was twice as small as the dystrophic one. Moreover, the most structured spots in the DMD tissue sections also exhibited a relatively low C18:1/C18:2 ratio value (1.09 and 1.20 for spot 1 of DMD sections 3 and 4, respectively), corroborating the healthier state of the cells in these areas.

ToF-SIMS imaging of PIs and TGs

In the negative ion mode, Touboul et al. (5) localized PI fragments, at m/z 223.0 and 241.0, together with TGs and fatty acid carboxylate ions, in the degenerating area of *mdx* mouse muscle sections. Their observation suggested that the fatty acid carboxylate ions could originate not only from free fatty acids but also from TG fragmentations, as observed previously by ESI-MS (30, 31), CF-LSIMS (32), and FAB-MS (33).

For the human samples, the PI fragment ions were present in all mass spectra, together with ions at m/z 259.0 and 299.0 (two other PI characteristic fragments) (34) and with the C20:4 ion at m/z 303.2 (Fig. 7B). The individual mass spectra of ROIs revealed a maximal abundance of these ions within the cells, indicating the presence of PIs, in particular PI38:4 (m/z 885.6), which contains a C20:4 fatty acyl chain (11, 35). PI and TG ions are observed together in the mass spectrum region m/z 760–920 (Fig. 7C), with characteristic series differing by 28 mass units (two methylene groups) and/or 2 mass units (one double bond). Their assignments are based, first, on the fact that TG ions

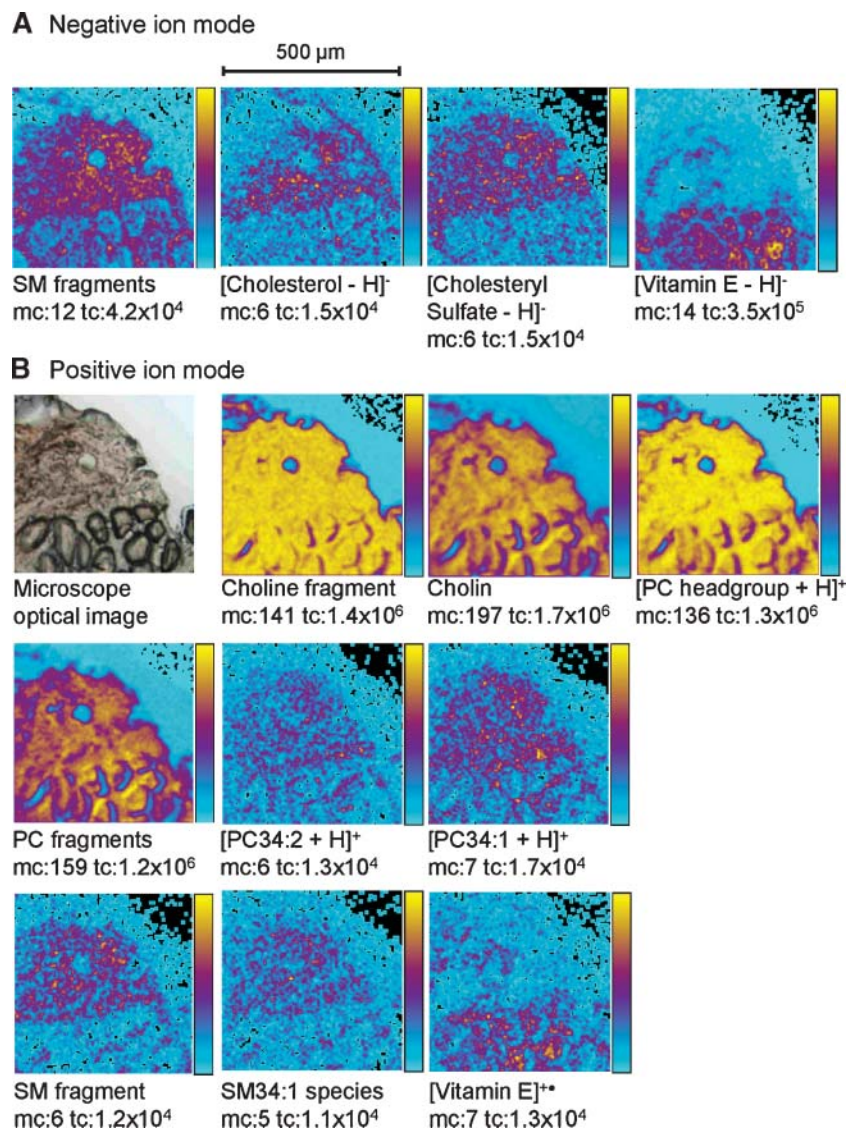


Fig. 8. ToF-SIMS ion images of spot 3 (see Fig. 1B). Below each ion image is the name of the selected species, with maximal number of counts in a pixel (mc) for the color scale and image total number of counts (tc). Some images are the result of the sum of several ion images, after verification of their exact colocalization. A: Negative ion mode. From left to right: sum of the SM fragment ion (m/z 616, 642, and 687); cholesterol; cholesteryl sulfate; and vitamin E deprotonated molecule. B: Positive ion mode. First line from left to right: microscope image; choline fragment (m/z 86); protonated choline molecule (m/z 104 ion image); and PC head group (m/z 184 ion image). Second line from left to right: PC fragments (sum of m/z 125, 166, 206, 224, and 246 ion images); m/z 758 ion image; and 760 ion image. Third line from left to right: SM fragment (m/z 668); sum of SM protonated and sodiated species (m/z 703 and 725); and vitamin E molecular ion.

are only detected in adipose or DMD-damaged tissues, and second, on the localization similarity between PI38:4, on the one hand, and PI34:0, PI36:2, PI36:1, and the PI fragments, on the other hand. Finally, the mass calculation can differentiate a PI ion from a TG ion, because the decimal part of a PI ion mass must be between 0.5 and 0.6, whereas the decimal part of a TG ion is between 0.7 and 0.8. Therefore, the ions at m/z 831.8 and 857.8 can only be TG50:1 and TG52:2, respectively. The ion at m/z 797.7 remains, as far as we know, unidentified.

The relative intensities of these ions varied, and in general, the more the cells were structured, the less the TGs

were present, in favor of the PIs. To obtain more details, we examined different ROIs to distinguish the different corresponding distributions. As an example, **Fig. 9A** displays the mass spectra obtained in the negative ion mode of the three ROIs selected in spot 3 (cells in red, damaged area in green, and adipocytes in blue). These spectra were spectacularly different. The images of the major ion peaks (Fig. 9B) led us to distinguish, on a molecular basis, the three regions of interest. The mass spectrum of the blue ROI showed the characteristic signals of TG ions (m/z 803.8, 805.8, 827.8, 829.8, 831.8, 833.8, 853.8, 855.8, 857.8, 859.8, 881.8, and 883.8), confirming the lipid-storing

TABLE 2. R_2 ratios calculated for each control and dystrophic spot

Sample	Section Number	Spot Number	Spot Ratio R_2	Section Average Value	SD	Sample Average Value	SD
DMD child 1	1	1	0.41	0.42	± 0.17	0.54	± 0.14
		2	0.66				
		3	0.30				
		4	0.29				
	2	1	0.44	0.62	± 0.12		
		2	0.73				
		3	0.58				
		4	0.66				
		5	0.54				
		6	0.76				
DMD child 2	3	1	0.70	0.50	± 0.14		
		2	0.42				
		3	0.45				
		4	0.57				
		5	0.35				
	4	1	0.73	0.59	± 0.09		
		2	0.52				
		3	0.50				
		4	0.52				
		5	0.60				
Control	1	1	1.09	0.75	± 0.12		
		2	0.65				
		3	0.75				
		4	0.77				
		5	0.50				
	2	1	0.63	0.63	± 0.00		
		2	0.63				
	3	1	0.88	0.88	± 0.04		
		2	0.92				
		3	0.84				
	4	1	0.72	0.77	± 0.12		
		2	0.91				
		3	0.69				

$R_2 = I_{m/z\ 283}/I_{m/z\ 281}$; ratio of the corrected intensity of the C18:0 fatty acid carboxylate signal at m/z 283.2 over the intensity of the C18:1 fatty acid carboxylate signal at m/z 281.2. Data originate from negative ion mode ToF-SIMS analyses of four human striated muscle sections from a control child and two sections from two DMD-affected children. The spots correspond to areas over which ToF-SIMS imaging experiments were carried out.

function of the adipocytes. Additionally, the presence of some of these species in the damaged area suggests that myofibers develop into adipocytes, in accordance with what has been observed in the degenerating areas of the *mdx* mouse model and in human dystrophic muscle tissue (36). By contrast, the peaks at m/z 835.6, 837.6, and 863.6 (Fig. 9A, red spectrum) can only originate from the PIs PI34:1, PI34:0, and PI36:1, respectively, but not from TGs. The colocalization of the peak at m/z 885.5 with these latter ions led us to assign this ion peak to the PI38:4 species and not the TG54:2 molecule and to assign the peak at m/z 861.6 to PI36:2 and not to TG52:0. All images corresponding to these PI38:4 and PI36:2 ions were perfectly superimposed with the localization of the cells (red ROI). Finally, three ion peaks at m/z 795.7, 797.7, and 799.7 were detected selectively in the damaged surface. Their absence in the adipocytes and in the cells suggested that they did stem from either TGs or PIs.

DISCUSSION

Dystrophin deficiency generates malfunctioning in the muscle cell membranes, as the transmembrane complex is largely destabilized, deregulating functional ion channels

and oxidation reaction cycles (1). Consequently, the absence of dystrophin and of its interactions with the membrane lipids induces membrane degeneration and muscle apoptosis or necrosis. Cell membrane dysfunction results in modifications of membrane lipid unsaturation as a consequence of disturbances in fatty acid metabolism (22). Because phospholipids are key components of muscle cell walls, the characterization of the degeneration/regeneration process, through the characterization of phospholipid composition and localization, is essential.

Glycerophosphatidylcholines are known to be a major component of muscle cell membrane phospholipids. These lipids bear a quaternary ammonium moiety granting a fixed positive charge that leads to higher signals than the other lipids present in the tissue, thereby facilitating their detection by mass spectrometry. MALDI-ToF profiling of the *mdx* mouse model has shown, in positive ion mode, the presence of PCs as the most abundant species in the region m/z 700–850, in particular PC34:2 and PC34:1 at m/z 758.6 and 760.6, respectively (4). In this lipid nomenclature (37), 34 represents the total number of carbons contained in the fatty acyl chains, with a total of two and one unsaturations, respectively. Under MALDI conditions, the intensity ratio of the ions at m/z 758.6 over 760.6 was found to be >1 in the pseudohealthy area of the *mdx*

TABLE 3. R_3 ratios calculated for each control and dystrophic spot

Sample	Section Number	Spot Number	Spot Ratio R_3	Section Average Value	SD	Sample Average Value	SD
DMD child 1	1	1	2.67	2.29	± 0.39	1.96	± 0.45
		2	1.74				
		3	2.41				
		4	2.33				
	2	1	2.74	2.06	± 0.46		
		2	1.86				
		3	2.46				
		4	1.77				
		5	2.03				
		6	1.52				
DMD child 2	3	1	1.09	1.76	± 0.46		
		2	1.62				
		3	2.15				
		4	1.71				
		5	2.22				
	4	1	1.20	1.79	± 0.43		
		2	1.93				
		3	2.25				
		4	1.50				
		5	2.08				
Control	1	1	0.74	0.99	± 0.18		
		2	1.18				
		3	1.03				
		4	0.88				
		5	1.14				
	2	1	1.00	0.93	± 0.11		
		2	0.85				
	3	1	0.78	0.96	± 0.29		
		2	0.81				
		3	1.30				
	4	1	0.92	1.01	± 0.17		
		2	0.90				
		3	1.21				

$R_3 = I_{m/z\ 281}/I_{m/z\ 279}$; ratio of the corrected intensity of the C18:1 fatty acid carboxylate signal at m/z 281.2 over the intensity of the C18:2 fatty acid carboxylate signal at m/z 279.2. Data originate from negative ion mode ToF-SIMS analyses of four human striated muscle sections from a control child and on two sections from two DMD-affected children. The spots correspond to areas over which ToF-SIMS imaging experiments were carried out.

mouse muscle and <1 in its destructured area. Healthy and dystrophic *mdx* mouse cultured cells exhibited a ratio value of >1 at the stage of myoblasts and of <1 after cell fusion in myotubes. This suggested that the destructured areas in the *mdx* muscle were actually undergoing a regeneration process rather than degeneration. Likewise, ToF-SIMS spectra of *mdx* mouse leg tissue sections also revealed PCs as the most abundant species in the region m/z 700–850 (5). However, the poor contrast of the ToF-SIMS images of intact PCs did not provide spatial information; thus, the composition modification revealed by MALDI-ToF could not be confirmed. Earlier studies (21, 22) have also shown that membrane PCs of the human dystrophic muscle incorporated less C18:2 fatty acyl chains than the healthy muscle, but more C18:1 and C18:0.

Although these experiments were performed with different samples and methods (i.e., mouse by MALDI-ToF and human by ToF-SIMS), the analyses can be qualitatively compared. Indeed, the control samples generally exhibited an R_1 almost twice as large as the DMD-affected samples, and the regenerating areas generated lower ratios. Thus, these ratios followed the same trends as in the *mdx* mouse model, in which ratio values were >1 for the control zones but <1 for the destructured (regenerating)

areas. As an example, Fig. 8 depicts the images of selected ions and their accumulation over spot 3. These images reveal that, in the DMD-affected muscle, the typical PC fragments colocalize with the parent species PC34:2 and PC34:1 (Fig. 8B), concentrated mainly in the dystrophic damaged region, as mentioned above. The specific localization and the absence of these phosphocholine species in the adipocytes and between the cells, where the low PC concentration is known, confirmed that our sample treatment did not induce any significant molecular delocalization.

PC, cholesterol, and SM colocalization

Cholesterol is a versatile essential membrane component involved in steroid hormone production and cell signaling (38), membrane structure and function (39), and synapse formation (40). PC fragments and cholesterol have been found to have a complementary distribution in the rat cerebellum (26) and in capillary blood leukocytes (41). Cholesteryl sulfate ions have been identified in ToF-SIMS imaging of human skin and renal human samples from a patient with a genetic disease (16). In agreement with this, the results obtained by ToF-SIMS imaging of the human control sample showed a complementary distribu-

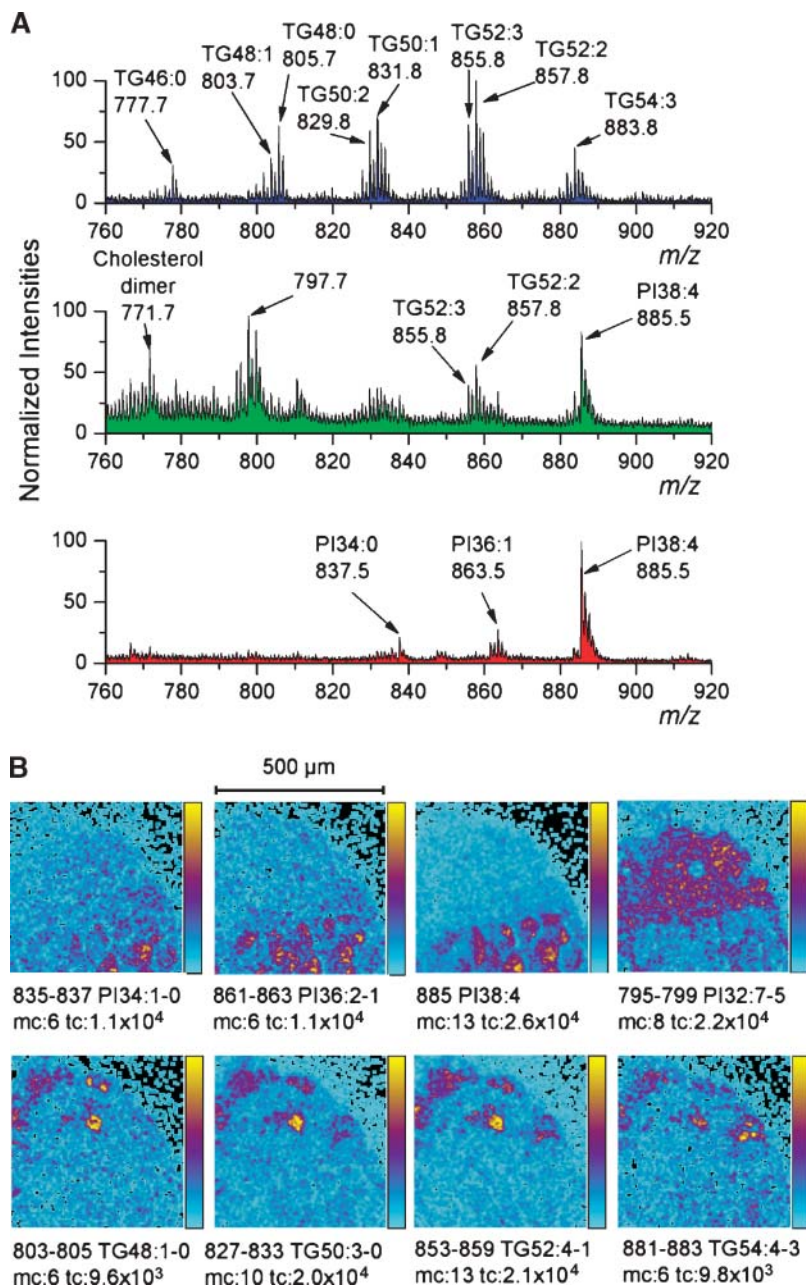


Fig. 9. ToF-SIMS analysis of spot 3 (see Fig. 1B) in negative ion mode. A: Mass spectra (m/z 760–920) of each of the selected ROIs. B: Ion images of the corresponding detected ions, with the mass range and class of affiliation (number of unsaturations) of the selected species, with maximal number of counts in a pixel (mc) for the color scale and image total number of counts (tc). PI, phosphatidylinositol.

tion of cholesterol, found in intercellular or adipocyte regions (data not shown), and PCs, mainly found within the cells. In contrast, cholesterol, cholesteryl sulfate (Fig. 8A), and intact PCs (Fig. 8B) colocalized in the damaged or intercellular regions of the DMD-affected samples. This has not been observed explicitly with the mouse samples. Hence, the colocalization might originate from a perturbation of the lipid regulation mechanisms, directly or indirectly inducing, in the human dystrophic muscle, a modification of the PC accumulation.

The three SM ion peaks presented in Fig. 7A appeared in all positive ion mass spectra of the DMD-affected sam-

ples, whereas they were quasi-absent in the mass spectra of healthy samples. Negative ion mass spectra showed that both control and DMD-affected muscles contained specific SM34:1 fragment ions (data not shown). However, it was substantially more abundant in the dystrophic samples, and increased with the extent of the damage, than in the control samples. These observations suggest that DMD-affected cells might develop a high sphingomyelinase activity induced by a disorder in the regulation of membrane sphingolipid composition. In healthy cells, after stress or apoptotic stimuli, sphingomyelinase is activated. This diminishes the level of SM converted into ceramide (a

signaling molecule involved in cell differentiation, proliferation, and apoptosis), and the dysfunctioning of the ceramide-mediated apoptosis pathway induces high levels of SM (42). Ceramides (SM derivatives) are vital signaling substances for tumors, forming SM-rich vesicles, and are responsible for their proliferation and survival (43). Additionally, it has been shown that phospholipase C activity increases in dystrophic mouse muscle, together with an increase of SM and TGs (21, 44, 45). This enzyme converts PC species into DGs and phosphocholine, both precursors of SM and TG biosynthesis (46, 47). In agreement with this hypothesis, in the human dystrophic muscle, the observed increase of SM species in negative ion mode goes along with a decrease of PC species, in favor of DG-type fragments (emerging from DGs and/or TGs) in positive ion mode (data not shown). The above-cited SM species have been observed in cryopreserved human spermatozoa (48) and low and high density lipoproteins (49). Wiseman et al. (23) found higher levels of SM in cancerous human liver adenocarcinoma than in nontumorous tissue.

Cholesterol and SM colocalization in the dystrophic muscle are in agreement with the literature reports on human samples (27) and support our peak assignments. Yet, this is at odds with the *mdx* mouse data, in which cholesterol accumulated mainly in the degenerating region together with vitamin E. Additionally, control samples displayed, in positive ion mode, cholesterol peaks with a much lower intensity than vitamin E signals (Fig. 3), whereas DMD-affected sections exhibited similar or higher intensities for cholesterol signal than for vitamin E (data not shown). This is also consistent with previous findings on dystrophic muscles (50–52). Therefore, Cholesterol, PC, and SM colocalization, associated with a much higher proportion of cholesterol, might suggest a tentative regulation and/or regeneration behavior of these highly damaged regions in human DMD-affected muscles.

Fatty acyl chain composition changes


ToF-SIMS analyses of the *mdx* mouse muscle (5) revealed a calculated C18:0/C18:1 ratio value six to seven times higher in the regenerating area than in the degenerating and control areas. In human samples, this ratio was only 1.5 times higher in the control spots than in the dystrophic spots (0.77 and 0.54, respectively). Additionally, in studies of mouse lipid fractions, a C18:2/C18:1 ratio value of 1.3 was reported for both healthy and predominantly nondestructured dystrophic myofilaments (51). As mentioned previously, this is probably attributable to the significantly low amount of destructured fibers and adipose and connective tissues in the dystrophic mouse muscle (1). Similarly, a lower incorporation of C18:2 in PCs has been observed in human dystrophic muscles, compared with healthy muscles, together with increased levels of C18:1 and C18:0 (21, 22). The variation of fatty acid composition between the different areas revealed in the present study can be interpreted as an attempt to stabilize the dystrophic cells, because the incorporation of saturated fatty acids in cell wall phospholipids reduces membrane flexibility. By contrast to the cells, the more damaged

zones of the DMD tissues showed an increased relative abundance of monounsaturated fatty acids (C18:1), as deduced from lower R_2 and higher R_3 values. Concerning the arachidonic acid carboxylate ions (C20:4), the distribution was found to be maximal in the degenerating zone. This fatty acid is, among others, a prostaglandin precursor that can accumulate in dystrophin-deficient muscles during inflammation.

PIs

The reduced relative abundance of the PI36:2 and PI36:1 compounds (m/z 861.6 and 863.6, respectively), with regard to the control tissue (Fig. 7C), might already hint at an increase of phospholipase activity in the DMD-affected muscle cells. The PI cycle rate is known to be reduced in dystrophic muscle cells, inducing high local phospholipase A₂, C, and D activities (53, 54). As mentioned above, the decrease of PIs is accompanied by an increase of TGs and SM, supporting the hypothesis of an enhanced phospholipase C activity. This increased activity is thought to be induced by the high concentration of intracellular calcium.

Conclusion

In summary, cluster-ToF-SIMS imaging allowed us to directly and relatively rapidly probe intact biological tissue sections with complete preservation of the sample molecular and structural integrity, a simultaneous analysis of different morphological regions at a micrometer scale and with high molecular specificity and sensitivity, without any prior preparation procedure. The specific localization of the different compounds in the positive ion mode imaging and its confirmation in the negative ion mode demonstrated the absence of any molecular delocalization at the micrometer scale on the samples. Moreover, the association of the mass spectra with images was highly useful, providing, on the one hand, molecular composition even when the image contrast was low, and on the other hand, spatial localization even with a low signal-to-noise ratio. ToF-SIMS imaging thus gives a considerable amount of information on the local molecular composition within tissues or organs and can be recognized as a powerful approach for localized lipidomics studies. This method emerges as a promising and highly valuable indicator of the disturbance of regulation processes, like the alteration of phospholipid incorporation or lipase dysfunction, paving the way for substantial assistance in drug design studies or the development of specific inhibitors. 

The authors thank the French Banque de Tissus pour la Recherche (Institut de Myologie) for providing surgery residues of human paravertebral striated muscles. The Banque de Tissus pour la Recherche is a partner of the EuroBioBank network funded by the European Commission under the Fifth Framework Programme (Grant QLRI-CT-2002-02769). N.T. is indebted to the Institut de Chimie des Substances Naturelles (Centre National de la Recherche Scientifique) for a postdoctoral grant. This work was supported by the European Union (Contract LSHG-CT-2005-518194 COMPUTIS).

REFERENCES

- Blake, D. J., A. Weir, S. E. Newey, and K. E. Davies. 2002. Function and genetics of dystrophin and dystrophin-related proteins in muscle. *Physiol. Rev.* **82**: 291–329.
- Voisin, V., C. Sebrie, S. Matecki, H. Yu, B. Gillet, M. Ramonaxo, M. Israel, and S. De La Porte. 2005. L-Arginine improves dystrophic phenotype in *mdx* mice. *Neurobiol. Dis.* **20**: 123–130.
- Bulfield, G., W. G. Siller, P. A. Wight, and K. J. Moore. 1984. X chromosome-linked muscular dystrophy (*mdx*) in the mouse. *Proc. Natl. Acad. Sci. USA.* **81**: 1189–1192.
- Touboul, D., H. Piednoel, V. Voisin, S. De La Porte, A. Brunelle, F. Halgand, and O. Lapr evote. 2004. Changes of phospholipid composition within the dystrophic muscle by matrix-assisted laser desorption/ionization mass spectrometry and mass spectrometry imaging. *Eur. J. Mass Spectrom.* **10**: 657–664.
- Touboul, D., A. Brunelle, F. Halgand, S. De La Porte, and O. Lapr evote. 2005. Lipid imaging by gold cluster time-of-flight secondary ion mass spectrometry: application to Duchenne muscular dystrophy. *J. Lipid Res.* **46**: 1388–1395.
- Brunelle, A., D. Touboul, and O. Lapr evote. 2005. Biological tissue imaging with time-of-flight secondary ion mass spectrometry and cluster ion sources. *J. Mass Spectrom.* **40**: 985–999.
- Touboul, D., F. Kollmer, E. Niehuis, A. Brunelle, and O. Lapr evote. 2005. Improvement of biological time-of-flight-secondary ion mass spectrometry imaging with a bismuth cluster ion source. *J. Am. Soc. Mass Spectrom.* **16**: 1608–1618.
- Nygren, H., C. Eriksson, P. Malmberg, H. Sahlin, L. Carlsson, J. Lausmaa, and P. Sj ovall. 2003. A cell preparation method allowing subcellular localization of cholesterol and phosphocholine with imaging TOF-SIMS. *Colloids Surf. B.* **30**: 87–92.
- Ostrowski, S. G., C. T. Van Bell, N. Winograd, and A. G. Ewing. 2004. Mass spectrometric imaging of highly curved membranes during *Tetrahymena* mating. *Science.* **305**: 71–73.
- Touboul, D., F. Halgand, A. Brunelle, R. Kersting, E. Tallarek, B. Hagenhoff, and O. Lapr evote. 2004. Tissue molecular ion imaging by gold cluster ion bombardment. *Anal. Chem.* **76**: 1550–1559.
- Sj ovall, P., J. Lausmaa, and B. Johansson. 2004. Mass spectrometric imaging of lipids in brain tissue. *Anal. Chem.* **76**: 4271–4278.
- Monroe, E. B., J. C. Jurchen, J. Lee, S. S. Rubakhin, and J. V. Sweedler. 2005. Vitamin E imaging and localization in the neuronal membrane. *J. Am. Chem. Soc.* **127**: 12152–12153.
- Nygren, H., K. B orner, P. Malmberg, E. Tallarek, and B. Hagenhoff. 2005. Imaging TOF-SIMS of rat kidney prepared by high-pressure freezing. *Microsc. Res. Tech.* **68**: 329–334.
- Nygren, H., K. B orner, P. Malmberg, and B. Hagenhoff. 2006. Localization of cholesterol in rat cerebellum with imaging TOF-SIMS—effect of tissue preparation. *Appl. Surf. Sci.* **252**: 6975–6981.
- Mas, S., D. Touboul, A. Brunelle, P. Aragoncillo, J. Egido, O. Lapr evote, and F. Vivanco. 2007. Lipid cartography of atherosclerotic plaque by cluster-TOF-SIMS imaging. *Analyst.* **132**: 24–26.
- Touboul, D., S. Roy, D. P. Germain, P. Chaminade, A. Brunelle, and O. Lapr evote. 2007. MALDI-TOF and cluster-TOF-SIMS imaging of Fabry disease biomarkers. *Int. J. Mass Spectrom.* **260**: 158–165.
- Veryovkin, I. V., S. F. Belykh, A. Adriaens, A. V. Zinovev, and F. Adams. 2004. On the trends in kinetic energies of secondary ions produced by polyatomic ion bombardment. *Appl. Surf. Sci.* **231–232**: 101–105.
- Gilmore, I. S., and M. P. Seah. 2000. Ion detection efficiency in SIMS: dependencies on energy, mass and composition for micro-channel plates used in mass spectrometry. *Int. J. Mass Spectrom.* **202**: 217–229.
- Touboul, D., A. Brunelle, and O. Lapr evote. 2006. Structural analysis of secondary ions by post-source decay in time-of-flight secondary ion mass spectrometry. *Rapid Commun. Mass Spectrom.* **20**: 703–709.
- B orner, K., H. Nygren, B. Hagenhoff, P. Malmberg, E. Tallarek, and J. E. M ansson. 2006. Distribution of cholesterol and galactosylceramide in rat cerebellar white matter. *Biochim. Biophys. Acta.* **1761**: 335–344.
- Pearce, P. H., R. D. Johnsen, S. J. Wysocki, and B. A. Kakulas. 1981. Muscle lipids in Duchenne muscular dystrophy. *Aust. J. Exp. Biol. Med.* **59**: 77–90.
- Kunze, D., G. Reichmann, E. Egger, D. Olthoff, and K. Dohler. 1975. Fatty acid pattern of lipids in normal and dystrophic human muscle. *Eur. J. Clin. Invest.* **5**: 471–475.
- Wiseman, J. M., S. M. Puolitaival, Z. Takats, R. G. Cooks, and R. M. Caprioli. 2005. Mass spectrometric profiling of intact biological tissue by using desorption electrospray ionization. *Angew. Chem. Int. Ed.* **44**: 7094–7097.
- Zhang, Y. H., M. R. Vasko, and G. D. Nicol. 2002. Ceramide, a putative second messenger for nerve growth factor, modulates the TTX-resistant Na(+) current and delayed rectifier K(+) current in rat sensory neurons. *J. Physiol.* **544**: 385–402.
- Titievsky, A., I. Titievskaya, M. Pasternack, K. Kaila, and K. Tornquist. 1998. Sphingosine inhibits voltage-operated calcium channels in GH4C1 cells. *J. Biol. Chem.* **273**: 242–247.
- Nygren, H., K. B orner, B. Hagenhoff, P. Malmberg, and J. E. M ansson. 2005. Localization of cholesterol, phosphocholine and galactosylceramide in rat cerebellar cortex with imaging TOF-SIMS equipped with a bismuth cluster ion source. *Biochim. Biophys. Acta.* **1737**: 102–110.
- Slotte, J. P. 1997. Cholesterol-sphingomyelin interactions in cells—effects on lipid metabolism. *Subcell. Biochem.* **28**: 277–293.
- Ohvo-Rekila, H., B. Ramstedt, P. Leppimaki, and J. P. Slotte. 2002. Cholesterol interactions with phospholipids in membranes. *Prog. Lipid Res.* **41**: 66–97.
- Ramstedt, B., and J. P. Slotte. 2002. Membrane properties of sphingomyelins. *FEBS Lett.* **531**: 33–37.
- Hsu, F. F., and J. Turk. 2000. Characterization of phosphatidylinositol, phosphatidylinositol-4-phosphate, and phosphatidylinositol-4,5-bisphosphate by electrospray ionization tandem mass spectrometry: a mechanistic study. *J. Am. Soc. Mass Spectrom.* **11**: 986–999.
- Stroobant, V., R. Rozenberg, E. M. Bouabsa, E. Deffense, and E. de Hoffmann. 1995. Fragmentation of conjugate bases of esters derived from multifunctional alcohols including triacylglycerols. *J. Am. Soc. Mass Spectrom.* **6**: 498–506.
- Li, C., and J. A. Yergey. 1997. Continuous flow liquid secondary ion mass spectrometric characterization of phospholipid molecular species. *J. Mass Spectrom.* **32**: 314–322.
- Murphy, R. C. 1993. Mass Spectrometry of Lipids (Handbook of Lipid Research, Vol. 7). Plenum Press, New York.
- Ostrowski, S. G., C. Szakal, J. Kozole, T. P. Roddy, J. Xu, A. G. Ewing, and N. Winograd. 2005. Secondary ion MS imaging of lipids in picoliter vials with a buckminsterfullerene ion source. *Anal. Chem.* **77**: 6190–6196.
- Wenk, M. R., L. Lucast, G. Di Paolo, A. J. Romanelli, S. F. Suchy, R. L. Nussbaum, G. W. Cline, G. I. Shulman, W. McMurray, and P. De Camilli. 2003. Phosphoinositide profiling in complex lipid mixtures using electrospray ionization mass spectrometry. *Nat. Biotechnol.* **21**: 813–817.
- Bonsett, C. A., and A. Rudman. 1994. ‘Oil globules’ in Duchenne muscular dystrophy—history, demonstration, and metabolic significance. *Med. Hypotheses.* **43**: 327–338.
- Fahy, E., S. Subramaniam, H. A. Brown, C. K. Glass, A. H. Merrill, Jr., R. C. Murphy, C. R. Raetz, D. W. Russell, Y. Seyama, W. Shaw, et al. 2005. A comprehensive classification system for lipids. *J. Lipid Res.* **46**: 839–861.
- Simons, K., and E. Ikonen. 2000. How cells handle cholesterol. *Science.* **290**: 1721–1726.
- Simons, K., and E. Ikonen. 1997. Functional rafts in cell membranes. *Nature.* **387**: 569–572.
- Pfriefer, F. W. 2003. Role of cholesterol in synapse formation and function. *Biochim. Biophys. Acta.* **1610**: 271–280.
- Sj ovall, P., J. Lausmaa, H. Nygren, L. Carlsson, and P. Malmberg. 2003. Imaging of membrane lipids in single cells by imprint-imaging time-of-flight secondary ion mass spectrometry. *Anal. Chem.* **75**: 3429–3434.
- Kolesnick, R. N., and M. Kronke. 1998. Regulation of ceramide production and apoptosis. *Annu. Rev. Physiol.* **60**: 643–665.
- Kim, C. W., H. M. Lee, T. H. Lee, C. Kang, H. K. Kleinman, and Y. S. Gho. 2002. Extracellular membrane vesicles from tumor cells promote angiogenesis via sphingomyelin. *Cancer Res.* **62**: 6312–6317.
- Kwok, C. T., and L. Austin. 1978. Phospholipid composition and metabolism in mouse muscular dystrophy. *Biochem. J.* **176**: 15–22.
- Banerjee, A. K., and S. Goyle. 1983. Altered lipid composition of adipose tissue in human muscular dystrophy. *Biochem. Med.* **30**: 246–252.
- Ullman, M. D., and N. S. Radin. 1974. The enzymatic formation of sphingomyelin from ceramide and lecithin in mouse liver. *J. Biol. Chem.* **249**: 1506–1512.
- Kanfer, J. N., and C. H. Spielvogel. 1975. Phospholipase C catalyzed

formation of sphingomyelin— ^{14}C from lecithin and N-(^{14}C)-oleoyl-sphingosine. *Lipids*. **10**: 391–394.

48. Schiller, J., J. Arnhold, H. J. Glander, and K. Arnold. 2000. Lipid analysis of human spermatozoa and seminal plasma by MALDI-TOF mass spectrometry and NMR spectroscopy—effects of freezing and thawing. *Chem. Phys. Lipids*. **106**: 145–156.
49. Schiller, J., O. Zschornig, M. Petkovic, M. Muller, J. Arnhold, and K. Arnold. 2001. Lipid analysis of human HDL and LDL by MALDI-TOF mass spectrometry and (^{31}P)-NMR. *J. Lipid Res.* **42**: 1501–1508.
50. Young, H. L., W. Young, and I. S. Edelman. 1959. Electrolyte and lipid composition of skeletal and cardiac muscle in mice with hereditary muscular dystrophy. *Am. J. Physiol.* **197**: 487–490.
51. Owens, K., and B. P. Hughes. 1970. Lipids of dystrophic and normal mouse muscle: whole tissue and particulate fractions. *J. Lipid Res.* **11**: 486–495.
52. Logan, D. M., and K. H. Tsang. 1992. Cholesterol alterations in young dystrophic mice. *Mol. Cell. Biochem.* **110**: 55–64.
53. Rounds, P. S., A. B. Jepson, D. J. McAllister, and J. L. Howland. 1980. Stimulated turnover of phosphatidylinositol and phosphatidate in normal and Duchenne-dystrophic human skin fibroblasts. *Biochem. Biophys. Res. Commun.* **97**: 1384–1390.
54. Liberona, J. L., J. A. Powell, S. Shenoi, L. Petherbridge, R. Caviedes, and E. Jaimovich. 1998. Differences in both inositol 1,4,5-trisphosphate mass and inositol 1,4,5-trisphosphate receptors between normal and dystrophic skeletal muscle cell lines. *Muscle Nerve*. **21**: 902–909.